An Atmospheric Radiosounding Database for Generating Land-Surface-Temperature Algorithms

Joan M. Galve, César Coll, Vicente Caselles, and Enric Valor

***Abstract*—A database of global, cloud-free, and atmospheric radiosounding profiles was compiled with the aim of simulating radiometric measurements from satellite-borne sensors in the thermal infrared. The objective of the simulated data is to generate split-window (SW) and dual-angle (DA) algorithms for the retrieval of land surface temperature (LST) from Terra/Moderate Resolution Imaging Spectroradiometer (MODIS) and Envisat/Advanced Along Track Scanning Radiometer (AATSR) data. The database contains 382 radiosounding profiles acquired over land, with nearly uniform distribution of precipitable water between 0.02 and 5.5 cm. Radiative transfer calculations were performed with the MODTRAN 4 code for six viewing angles between 0° and 60°. The resulting radiance spectra were convoluted with the response filter functions of MODIS bands 31 and 32 and AATSR channels at 11 and 12 μm. By using the simulation database, the SW algorithms adapted for MODIS and AATSR data and the DA algorithms for AATSR data were developed. Both types of algorithms are quadratic in the brightness-temperature difference and depend explicitly on the land surface emissivity. The SW and DA algorithms were validated with actual ground measurements of LST collected concurrently to MODIS and AATSR observations in a site located close to the city of Valencia, Spain, in a large, flat, and thermally homogeneous area of rice crops. The results obtained have no bias and a standard deviation around ±0.5 K for the SW algorithms at nadir for both sensors. The SW algorithm used in the forward view results in a bias of 0.6 K and a standard deviation of ±0.8 K. The worst results are obtained in the other algorithms with a bias close to −1.0 K and a standard deviation close to ±1.1 K in the case of the DA algorithms.**

***Index Terms*—Advanced Along Track Scanning Radiometer (AATSR), land surface temperature (LST), Moderate Resolution Imaging Spectroradiometer (MODIS), radiative transfer simulation.**

I. Introduction

LAND SURFACE temperature (LST) is one of the most important inputs for studying the energy and mass balance between the surface and the atmosphere. In particular, LST is needed in meteorological prediction models [3], [18], in retrieving evapotranspiration through satellite data [11], [34], [44], in the evaluation of frost damage in crops [9], and in wildfire detection [8], [23]. Moreover, LST is considered an indicator of global change [2] and desertification [22]. Thermal-infrared (TIR) remote sensing is the unique way to obtain the LST of large land areas with different spatial resolutions and periodicities.

The derivation of LST from TIR satellite data requires the correction for atmospheric and emissivity effects. More than 20 years of research have shown that split-window (SW) methods can be operationally used for the retrieval of accurate LSTs. The SW methods use two spectral channels, which are usually at 11 and 12 μm, and have been applied to NOAA/Advanced Very High Resolution Radiometer (AVHRR) data [4], [6], [13], [31]. Currently, this technique is the basis of the LST operational products of the EOS Terra–Aqua/Moderate Resolution Imaging Spectroradiometer (MODIS) [42] and the Envisat/Advanced Along Track Scanning Radiometer (AATSR) [30]. It is also proposed for future sensors such as the Visible Infrared Imaging Radiometer Sensor [45].

SW methods are physically based on the differential absorption principle [24], which is also applicable for TIR measurements performed over the same target at two different observation angles, which are typically nadir and off-nadir. These are the so-called dual-angle (DA) methods. Both the SW and DA methods express the LST as a linear or quadratic combination of the brightness temperatures in the considered spectral channels or viewing angles, with constant coefficients having global validity. Coefficients could depend explicitly on surface emissivity (usually, the mean emissivity and the emissivity difference in the channels/angles are used), or different coefficient sets are given for each land-cover type. The determination of the algorithm coefficients usually relies on the use of simulated brightness temperatures. A set of atmospheric profiles representative at global scale and a radiative transfer model are used to predict the measurements of the satellite sensor for different prescribed surface temperatures and emissivities. A regression analysis of LST against the simulated brightness temperatures and emissivities according to a predetermined model equation yields the coefficients (e.g., [6] and [41]). Other approaches use actual brightness temperatures with concurrent ground measurements of LST (matchups) to derive the coefficients [20], [28], [29]. However, due to the limited number of matchups used, these coefficients have only local validity.

The coefficients obtained in the simulation procedure depend closely on the database of atmospheric profiles used in the simulation. Atmospheric profiles could be standard atmospheres, synthetic profiles (i.e., reanalysis data), or actual radiosounding measurements. Anyhow, the profile database should cover the global variability of the atmosphere as much as possible. In the

Manuscript received April 12, 2007; revised October 2, 2007. This work was supported in part by the Ministerio de Educación y Ciencia under Project CGL2004-06099-C03-01 and in part by the European Union FEDER funds, acciones complementarias under Project CGL2005-24207-E and Project CGL2006-27067-E. The work of J. M. Galve was supported by AQ1

The authors are with the Department of Earth Physics and Thermodynamics, Faculty of Physics, University of Valencia, 46100 Valencia, Spain (e-mail: joan.galve@uv.es).

Digital Object Identifier 10.1109/TGRS.2008.916084

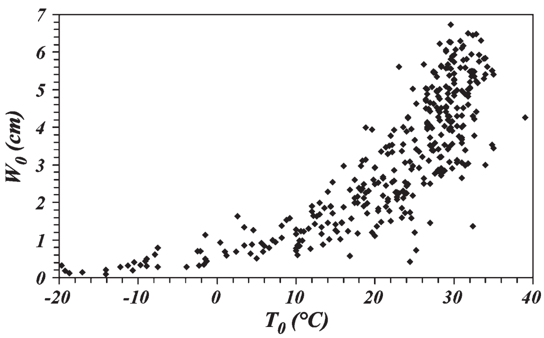

Fig. 1. Plot of T_0 versus W_0 for the CLAR database rasiosoundings.

case of marine atmospheres and for derivation of sea surface temperature algorithms, the SAFREE radiosounding database [16] includes 402 cloud-free actual radiosoundings. It has a good latitudinal distribution, and the vertical column water vapor (W_0) distribution is uniform up to 3.5 cm and has values up to 5 cm. The first-layer temperatures are comprised from close to 0 °C to around 30 °C. The first aim of this paper is to compile a database with similar characteristics in the case of land atmospheres. This database must be cloud-free, composed of actual atmospheric profiles taken over land, equally distributed in latitude, and with good temperature and W_0 distribution, as shown in Fig. 1. This database is named Cloudless Land Atmosphere Radiosounding (CLAR).

The second aim of this paper is to generate LST retrieval algorithms from the CLAR database simulations. We focused on the Terra/MODIS and Envisat/AATSR sensors. MODIS bands 31 (10.78–11.28 μm) and 32 (11.77–12.27 μm) are suitable for the SW algorithm. Then, we generated one MODIS SW (MSW) algorithm. The AATSR channels at 11 and 12 μm can also be used for the SW algorithms. In addition, the scanning concept of AATSR allows the observation of the same target at two viewing angles. First, it is observed off-nadir ($\sim$55°) in the so-called forward view. About 120 s later, the target is observed at nadir ($< 23°$) in the nadir view. Therefore, we have generated two AATSR SW algorithms for each view (ASWn for the nadir view and ASWf for the forward view) and two DA algorithms for each channel (ADA11 for the 11-μm channel and ADA12 for the 12-μm channel).

This paper is organized as follows. Section II presents the CLAR database, the simulation methodology, and the parameterization. Section III shows the theoretical model and the different LST algorithms generated. A sensitivity analysis of these algorithms with their error sources is presented in Section IV. In Section V, the algorithms are validated in a flat thermally homogeneous crop-field validation site to estimate the accuracy of the algorithms in real conditions. Finally, the conclusion is given in Section VI.

II. CLAR Database

The CLAR database was constructed with atmospheric radiosoundings compiled from the Atmospheric Science Department, University of Wyoming (http:// weather.uwyo.edu/upperair/sounding.html). It contains 382 global land atmospheric radiosoundings acquired at day and night times and uniformly distributed at the global scale. CLAR has a good distribution in W_0 which is uniform up to 5.5 cm and extends up to nearly 7 cm. The sondes are distributed in three latitude ranges, with around 40% of radiosoundings placed at low latitudes (0°–30°), another 40% at middle latitudes (30°–60°), and 20% at high latitudes ($> 60°$). The temperature of the first layer of the radiosoundings (T_0) ranges from -20 °C to 40 °C. All radiosoundings were taken from 2003 to 2006 and were checked by means of a cloud test in order to be sure that no cloud was included. François *et al.* [16] considered that a radiosounding was cloudy when it had a level with a relativity humidity (RH) higher than 85% or 80% depending on the latitude. Since maritime aerosols are salt based, more condensation occurs for lower RH in sea atmospheres than in land atmospheres. Therefore, we can consider a more relaxed RH threshold. Then, a radiosounding was considered cloudy when one layer had an RH larger than 90% or when two consecutive layers had an RH $> 85\%$. A radiosounding was considered foggy, and then rejected, when it had an RH $> 80\%$ within the two first kilometers. The CLAR database is available upon request to the authors.

Each radiosounding of CLAR was introduced into the multilayer radiative transfer model MODTRAN 4 [7], which is distributed in 65 layers from ground level to 100 km. Seasonal rural aerosol profile was assumed, with 24 km of visibility, and standard profiles of fixed gases were used in the simulations for each radiosounding. Atmospheric transmittance $\tau_\lambda(\theta)$ and upward and downward atmospheric radiances $L_\lambda^\uparrow(\theta)$ and $L_\lambda^\downarrow(\theta)$ were simulated for a wavenumber interval from 600 to 3000 cm^{-1} (16.6–3.3 μm) in steps of 2 cm^{-1}. Six at surface observation angles θ were selected to simulate the transmittance and the upward radiance. Wan and Dozier [40] proposed the use of Gaussian angles (11.6°, 26.1°, 40.3°, and 53.7°) for their good distribution. In this paper, we added nadir (0°) and 65° for completeness. The downwelling radiance was simulated also for the Gaussian angles, plus 0°, 65°, 70°, 80°, 85°, and 89° for a better description at larger angles. The sky downwelling irradiance $F_{\mathrm{sky},\lambda}^\downarrow$ was calculated as

$$F_{\mathrm{sky},\lambda}^\downarrow = \int_0^{2\pi}\int_0^{\pi/2} L_\lambda^\downarrow(\theta)\sin\theta\cos\theta \mathrm{d}\theta\mathrm{d}\varphi. \tag{1}$$

In order to select a surface temperature T according to the radiosounding first-layer air temperature T_0, several authors proposed different intervals. For example, Yu *et al.* [45] took $T_0 - 15 \leq T \leq T_0 + 15$; Ouaidrari *et al.* [26] took $T_0 - 10 \leq T \leq T_0 + 20$; Pinheiro *et al.* [27] took $T_0 - 16 \leq T_0 \leq T_0 + 16$; and Wan and Dozier [40] took $T_0 - 20 \leq T_0 \leq T_0 + 20$. In our case, we made a statistical study of the difference between the first-layer temperature (obtained through product MOD08 which is a global eight-day collection of atmospheric-profile retrieval MODIS product [35]) and the LST [obtained through global eight-day LST and emissivity MODIS products (MOD11, [42])] for 2005 to estimate a realistic difference $\Delta T = (T - T_0)$. Forty-five different scenes were taken. In each image, only land and cloud-free pixels were taken into

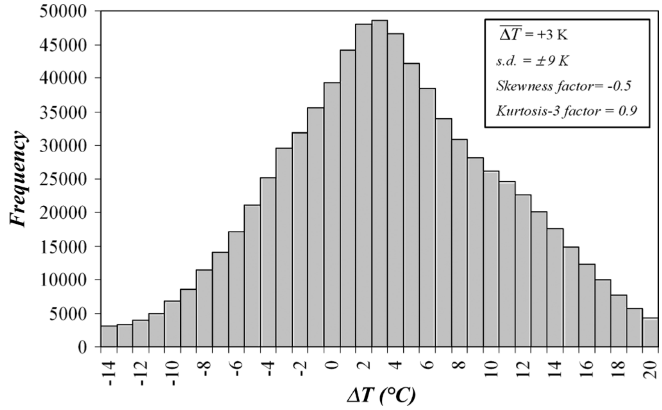

Fig. 2. Histogram distribution of global $\Delta T = T - T_0$ for 2005. T is the LST obtained through an eight-day global LST MODIS product (MOD11, [42]). T_0 is the temperature of the first-layer atmospheric profile obtained through an eight-day global atmospheric profile product (MOD08, [35]).

account. Fig. 2 shows the histogram distribution of this difference. The mean difference is $\overline{\Delta T} = +3$ K, and the standard deviation is ± 9 K. Therefore, we selected $T = T_0 - 6$, $T_0 - 2$, $T_0 + 1$, $T_0 + 3$, $T_0 + 5$, $T_0 + 8$, and $T_0 + 12$ following a Gaussian distribution.

III. SW and DA Algorithms for LST

In this section, we describe the theoretical model of Coll and Caselles [13] for LST retrieval. Later, this model is used with the CLAR database simulations to obtain the coefficients of the LST algorithms with their specific characteristics. Finally, the algorithms obtained for AATSR and MODIS are presented.

A. Theoretical SW Model of Coll and Caselles (1997)

Starting from the radiative transfer equation applied to satellite-sensor measurements, assuming Lambertian surface reflection and linearizing the Planck function with respect to temperature, the SW model of Coll and Caselles [13] expresses the surface temperature (T) as

$$T = T_1 + \Delta + A(T_1 - T_2) + \alpha(1 - \varepsilon) - \beta\Delta\varepsilon \qquad (2)$$

where the inputs are the brightness temperatures T_i ($i = 1$ and 2 being the channels at 11 and 12 μm, respectively) and the surface emissivity through the mean emissivity $\varepsilon = (\varepsilon_1 + \varepsilon_2)/2$ and the emissivity difference $\Delta\varepsilon = \varepsilon_1 - \varepsilon_2$ in the two channels. It should be noted that (1) is also applicable to the DA algorithms if subindex $i = 1$ and 2 refer to nadir and off-nadir views, respectively. In (2), the atmospheric and emissivity effects on LST are decoupled through coefficients Δ and A (atmospheric correction coefficients) and α and β (emissivity correction coefficients). The coefficients of (2) are given by

$$A = \frac{1 - \tau_1(\theta)}{\tau_1(\theta) - \tau_2(\theta)} \qquad (3)$$

$$\Delta = -\left[1 - \tau_2(\theta)\right] A \left(T_{\mathrm{a1}}^{\uparrow} - T_{\mathrm{a2}}^{\uparrow}\right) \qquad (4)$$

which depend only on the atmosphere through the atmospheric transmittance $\tau_i(\theta)$ at observation angle θ and the effective atmospheric temperature in the upward direction $T_{\mathrm{a}i}^{\uparrow}$ (defined from the upward atmospheric radiance according to McMillin [24]). The emissivity coefficients are given by

$$\alpha = (b_1 - b_2)A\tau_2(\theta) + b_1 \qquad (5)$$

$$\beta = A\tau_2(\theta)b_2 + \alpha/2 \qquad (6)$$

with

$$b_i = \frac{T_i}{n_i} + \gamma_i\left(\frac{n_i - 1}{n_i}T_i - T_{\mathrm{a}i}^{\downarrow}\right)\left[1 - \tau_i(0^\circ)\right]. \qquad (7)$$

where $T_{\mathrm{a}i}^{\downarrow}$ is the effective atmospheric temperature in the downward direction [24], and γ_i is the ratio between the downwelling sky irradiance (1) and π times the at-nadir downward radiance $\gamma_i = F_{\mathrm{sky},i}^{\downarrow}/\pi L_i^{\downarrow}(0^\circ)$. Coefficient n_i is the exponent of the power law approximation for the channel averaged Planck function ($B_i(T) \approx k_i T^{\mathrm{ni}}$ [31]), which depends on the channel ($n_{31} = 4.618$ and $n_{32} = 4.248$ for MODIS channels 31 and 32 and $n_{11} = 4.686$ and $n_{12} = 4.248$ for AATSR channels at 11 and 12 μm). More details on the derivation of (2) can be found in [12].

B. AATSR and MODIS Algorithms

The theoretical expressions of the coefficients (3)–(7) cannot be used in an operational LST algorithm. Instead, we calculated the coefficients from brightness temperatures simulated from the CLAR database. As pointed out before, coefficients A and Δ depend only on the atmosphere but not on the surface emissivity. In addition, for a black-body surface ($\varepsilon = 1$ and $\Delta\varepsilon = 0$), (2) yields

$$T = T_1 + \Delta + A(T_1 - T_2). \qquad (8)$$

Therefore, coefficients A and Δ can be obtained from the regression of $T - T_1$ against $T_1 - T_2$, with the brightness temperatures simulated for the black-body case. According to Coll and Caselles [13], the regression should be quadratic rather than linear, which implies that coefficient A is a linear function of $T_1 - T_2$ and that Δ is a constant

$$A = a_1 + a_2(T_1 - T_2) \qquad (9)$$

$$\Delta = a_0 \qquad (10)$$

where a_0, a_1, and a_2 are the constant values for a particular channel or angular combination, and they are referred to as the atmospheric coefficients hereafter. They can be applied over any nonblack-body surface, provided that the emissivity effects are accounted for through coefficients α and β for which it is necessary to calculate b_i (7). These coefficients depend on the surface temperature and the atmospheric properties. They were calculated for the radiosoundings of the CLAR database for

TABLE I

COEFFICIENTS FOR b_i ESTIMATION (11) FOR ALL CHANNELS WITH THEIR STATISTICAL ERRORS. ADJUSTMENT ERROR (σ_b) AND CORRELATION COEFFICIENT (R^2) FOR EACH CHANNEL ARE SHOWN IN THE LAST TWO LINES

	AATSR				MODIS	
	$T_{11\,\mu m}$ nadir	$T_{11\,\mu m}$ forward	$T_{12\,\mu m}$ nadir	$T_{12\,\mu m}$ forward	T_{31} (11 μm)	T_{32} (12 μm)
M (cm^{-1})	0.1038±0.0009	0.132±0.0017	0.1205±0.0017	0.125±0.002	0.1063±0.0009	0.1213±0.0014
N	0.239±0.003	0.288±0.006	0.335±0.006	0.397±0.009	0.243±0.003	0.290±0.005
P (Kcm^{-1})	-38.9±0.3	-49.2±0.6	-46.3±0.6	-47.8±0.9	-39.9±0.4	-46.5±0.6
Q (K)	-6.9±1.2	-24±2	-34±2	-56±3	-7.3±1.2	-17.8±1.9
σ_b(K)	*3*	*5*	*6*	*9*	*4*	*6*
R^2	*0.987*	*0.953*	*0.912*	*0.858*	*0.979*	*0.918*

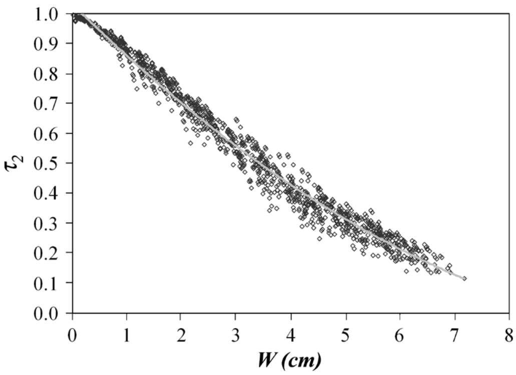

Fig. 3. Atmospheric transmittance τ_2 plotted against the path column water vapor content for the MODIS simulated data.

the surface temperatures corresponding to each profile. Then, the calculated coefficient b_i was parameterized in terms of T_i and W_0. It should be noted that in the cases of SW algorithms in nadir view, it is considered the path water vapor content $W = W_0/\cos\theta$. Taking this into account and according to Coll and Caselles [13], we can express b_i coefficients as

$$b_i = (M_i W + N_i)T_i + P_i W + Q_i \tag{11}$$

where coefficients M_i, N_i, P_i, and Q_i depend on the channel or view angle considered and were obtained from regression on the calculated b_i (see Table I). Finally, the transmittance τ_2 required for α and β [(5) and (6)] can be adjusted to a function of path or vertical water vapor content, depending on the algorithm generated, through a quadratic expression, as shown in Fig. 3

$$\tau_2 = t_0 + t_1 W + t_2 W^2 \tag{12}$$

where coefficients t_0, t_1, and t_2 depend on the channel/angle and were obtained from regression on the transmittances simulated in CLAR (see Table II).

Four different algorithms were generated for AATSR. In the nadir mode, viewing angles are $\theta < 23.5°$, and then, to generate ASWn, we used simulations at the observation angles: 0°, 11.6°, and 26.1°. ASWf was generated from simulations obtained only for 53.7°. The two AATSR DA algorithms were generated from simulations obtained for two pairs of observation angles: 0°–53.7° and 11.6°–53.7°, in the AATSR channels at 11 μm (ADA11) and 12 μm (ADA12).

Although MODIS at surface viewing angle reaches 65°, the algorithm for MODIS, the MSW, was generated from simulations obtained for the observation angles: 0°, 11.6°, 26.1°, and 40.3°. Since there are few studies on the angular variation of emissivity for land surfaces and due to the degradation of regression results for angles larger than 45°, in this paper, we have restricted to $\theta < 45°$ to generate the MSW algorithm.

With all these conditions, we can simulate sensor measurements for each algorithm. Thus, we have 2674 different cases for each geometrical configuration. Based on (2), and (8)–(10), all the algorithms generated can be expressed as

$$T = T_1 + a_0 + a_1(T_1 - T_2) + a_2(T_1 - T_2)^2 + \alpha(1-\varepsilon) - \beta\Delta\varepsilon. \tag{13}$$

The necessity of determining atmospheric correction coefficients (a_0, a_1, and a_2) is shown in Fig. 4, which plots the differences LST-T_1 versus the brightness-temperature differences $(T_1 - T_2)$ for the MSW case. A quadratic relationship between LST and $(T_1 - T_2)$ is clearly observed, which justifies the parameterization of coefficient A proposed in (9). Atmospheric coefficients with their errors, adjustment error (σ_{AC}) for all algorithms, and correlation coefficients (R^2) are shown in Table III. In order to evaluate the accuracy of these coefficients in different W_0 cases, we compare the temperature prescribed in the simulation T, with the LST obtained by applying (8)–(10) with the coefficients of Table III to all simulated cases. Fig. 5 shows the difference between T-LST in front of W_0. This shows that the algorithm works with better accuracy for atmospheres with low-to-moderate column water vapor content, the scattering being larger for $W_0 > 4$ cm.

Fig. 6 shows the values of α and β coefficients versus W for the atmospheric profiles and surface temperatures of the CLAR database. It shows that such coefficients have a clear dependence on the atmospheric moisture. Then, the α and β coefficients can be calculated through a simpler formulation in which only the dependence on the atmospheric water content W is considered. The coefficients α and β calculated from the CLAR radiosoundings and (5)–(7) can be approximated to

$$\alpha = \alpha_0 + \alpha_1 W + \alpha_2 W^2 \tag{14}$$

$$\beta = \beta_0 + \beta_1 W \tag{15}$$

where the coefficients depend on the combination of channels/angles used (see Table IV).

TABLE II
COEFFICIENTS FOR τ_2 ESTIMATION (12) FOR ALL ALGORITHMS WITH THEIR STATISTICAL ERRORS. ADJUSTMENT ERROR (σ_τ) AND CORRELATION COEFFICIENT (R^2) FOR EACH ALGORITHM ARE SHOWN IN THE LAST TWO LINES

	ASWn $T_{12\,\mu m}$ nadir	ASWf $T_{12\,\mu m}$ forward	ADA11 $T_{11\,\mu m}$ forward	ADA12 $T_{12\,\mu m}$ forward	MSW T_{32} (12 µm)
t_0	1.011±0.004	1.007±0.004	1.025±0.004	1.007±0.004	1.030±0.004
t_1	-0.187±0.003	-0.266±0.003	-0.184±0.003	-0.266±0.003	-0.170±0.003
t_2	0.0091±0.0004	0.0189±0.0005	0.0076±0.0005	0.0189±0.0005	0.0063±0.0005
σ_τ	*0.005*	*0.010*	*0.008*	*0.007*	*0.005*
R^2	*0.991*	*0.992*	*0.988*	*0.992*	*0.989*

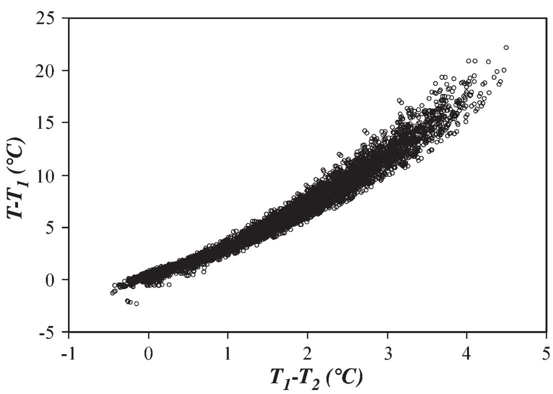

Fig. 4. Plot of $T - T_1$ versus the brightness-temperature difference $T_1 - T_2$ for the MSW case.

From this point, we can consider two alternative ways to obtain α and β, either with dependence on T_i and W or only on W. In version 1, coefficients α and β are obtained by using (5), (6), (11), and (12) and the coefficients for estimating b_i and τ_2 given in Tables II and III. In version 2, coefficients α and β are obtained by using (14) and (15) and the coefficients of Table IV.

IV. SENSITIVITY ANALYSIS

The accuracy of the algorithms is evaluated with a sensitivity analysis. The theoretical error of T is expressed as a combination of two main terms: one due to model accuracy $\delta(T)_\mathrm{M}$ and the other due to error propagation $\delta(T)_\mathrm{P}$

$$\delta(T) = \left[\delta(T)_\mathrm{M}^2 + \delta(T)_\mathrm{P}^2\right]^{1/2} \tag{16}$$

where

$$\delta(T)_\mathrm{M} = \left[\sigma_\mathrm{AC}^2 + [(1-\varepsilon)\sigma_\alpha]^2 + [\Delta\varepsilon\sigma_\beta]^2\right]^{1/2} \tag{17}$$

$$\delta(T)_\mathrm{P} = \left[\sum_i \left[\frac{\partial T}{\partial x_i}\delta x_i\right]^2\right]^{1/2}. \tag{18}$$

σ_AC is the error of atmospheric-correction-coefficient adjustment, and σ_α and σ_β are the errors of the α and β coefficient adjustments, respectively, which are weighted by the mean emissivity and the emissivity difference. The error-propagation inputs x_i are the brightness temperature, the emissivity and column water vapor content, and their respective errors (δx_i).

We have used the following values of the different variables to estimate the errors of (18). Brightness-temperature acquisition from on-board sensor has a noise equivalent difference of temperature (NEΔT), which is $\delta T_i = 0.05$ K for MODIS and AATSR [1], [37]. The variability of ε and $\Delta\varepsilon$ is the principal drawback to obtain the LST. In order to estimate the error associated to emissivity, different considerations have been made. First, different techniques can be used to assess the land surface emissivity from satellite-borne sensors, such as the temperature-emissivity-separation algorithms [17], AQ3 temperature-independent spectral-indices-based methodologies AQ4 [5], [25], or algorithms based on the use of vegetation indices [38], [39] among others. In all cases, emissivity can be assessed with an error around ±0.01 [10], which is a value that can be used for $\delta\varepsilon$ (and $\delta\Delta\varepsilon = \sqrt{2}\delta\varepsilon$). In addition, to estimate the error associated to these parameters, several ε and $\Delta\varepsilon$ values are used for each. Rubio *et al.* [32] measured emissivities for vegetated and soil samples. Emissivity varies from 0.942 to 0.991 for vegetation and from 0.903 to 0.997 for soils. Pinheiro *et al.* [27] estimated the emissivity values for AVHRR channels 4 and 5 for the FAO soil classes and vegetation types, showing that ε varies from 0.968 to 0.990 and $\Delta\varepsilon$ varies from -0.014 to 0.009. Since the AATSR channels are similar to AVHRR, these values can be used for the AATSR algorithms. In the case of MODIS, Snyder and Wan [36] obtained the emissivities for the International Geosphere–Biosphere Programme AQ5 classes, from which ε varies from 0.969 to 0.990 and $\Delta\varepsilon$ varies from -0.006 to 0.011. Then, for ASWn and MSW, we took five emissivity values, i.e., 0.970, 0.975, 0.980, 0.985, and 0.990, and five emissivity difference values, i.e., -0.01, -0.005, 0, 0.005, and 0.01. However, in the cases of ASWf, ADA11, and ADA12, an estimation of the directional variation of emissivity is needed. Snyder and Wan [36] obtained that ε and $\Delta\varepsilon$ vary in off-nadir view (~60°) from $\varepsilon = 0.969$ to 0.998 and from $\Delta\varepsilon = -0.007$ to 0.008. Then, for ASWf, we added one mean emissivity value $\varepsilon = 0.995$. The same values were used for ADA11 and ADA12.

Coefficients α and β calculated by using version 1 were compared with theoretical coefficients obtained by using (5)–(7). The resulting root-mean-square error (rmse) was compared with σ_α and σ_β of the adjustment of version 2 (Table IV). For coefficient α, the rmse of version 1 varies between 3 and 4 K in all algorithms in front of σ_α of version 2 that varies between 4 and 6 K. Coefficient β had a larger difference between both versions. The rmse of version 1 ranges from 6 K (ASWn, ASWf, and ADA11) to 10 K (ADA12 and MSW), and σ_β's for version 2 (Table IV) are 9 K for ASWn and ADA11, 11 K for ASWf, 13 K for ADA12, and 15 K for MSW. In order to estimate the effect of these errors in δT, we must choose the values of $\varepsilon = 0.980$ and $\Delta\varepsilon = 0.005$. Then, with these values

TABLE III
ATMOSPHERIC COEFFICIENTS WITH THEIR STATISTICAL ERRORS FOR ALL ALGORITHMS. ADJUSTMENT ERROR (σ_{AC}) AND CORRELATION COEFFICIENT (R^2) FOR EACH ALGORITHM ARE SHOWN IN THE LAST TWO LINES

	ASWn	**ASWf**	**ADA11**	**ADA12**	**MSW**
1	$T_{11\,\mu m}$ nadir	$T_{11\,\mu m}$ forward	$T_{11\,\mu m}$ nadir	$T_{11\,\mu m}$ nadir	T_{31} (11 μm)
2	$T_{11\,\mu m}$ nadir	$T_{12\,\mu m}$ forward	$T_{11\,\mu m}$ forward	$T_{12\,\mu m}$ forward	T_{32} (12 μm)
a_0 (K)	0.024±0.018	0.16±0.07	-0.059±0.012	-0.01±0.03	0.319±0.011
a_1	0.782±0.016	0.49±0.06	1.569±0.012	1.57±0.03	2.370±0.017
a_2 (K^{-1})	0.320±0.03	0.437±0.007	0.176±0.002	0.303±0.005	0.494±0.005
σ_{AC} (K)	*0.6*	*1.3*	*0.4*	*0.8*	*0.6*
R^2	*0.973*	*0.939*	*0.990*	*0.977*	*0.981*

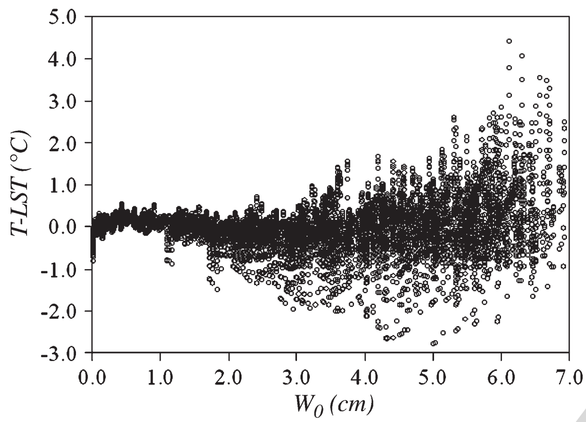

Fig. 5. Plot of T-LST versus the W_0 for the MSW case.

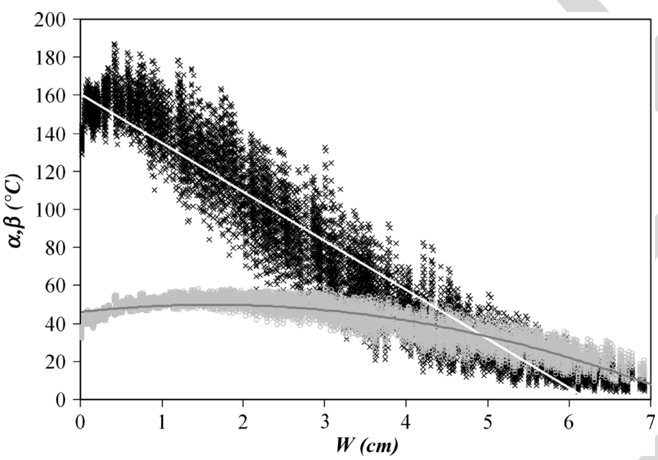

Fig. 6. (Gray circle) α and (black cross) β coefficients for the MSW algorithm against the path column water vapor content W (in centimeters).

and the errors of both versions previously given, we obtained $\delta T = \pm 0.09$ K for version 1 and $\delta T = \pm 0.12$ K for version 2. The difference between these two versions is less than the NEΔT (±0.05 K). Then, since there is no significant difference between them, we chose the version 2 of the algorithms for simplicity.

In order to evaluate the effect of all these error sources in different atmospheric conditions, they have been evaluated for different W's (1, 2, 3, 4, and 5 cm), considering a typical error of 10% [35]. However, this error may be underestimated for low W cases, for which an error of ±0.4 cm could be more realistic. Therefore, we estimated the error in temperature resulting from both cases of δW and selected the largest temperature error. For each W, different values of $T_1 - T_2$ and T_i must be taken into account for each algorithm. These are the typical values from the simulation of CLAR for the different W's considered. Table V shows the values taken.

Fig. 7 shows the error in LST due to the different sources in the case of MSW and ADA11. The other algorithms yielded similar results. The maximum error in LST for MSW is close to 2.1 K, and for ADA11, it is close to 1.6 K, decreasing with W in both cases. The main error source is emissivity; thus, a good knowledge of this quantity is necessary. The adjustment error of the coefficients, which is constant, is the other significant source of error. Finally, W and brightness temperature error are less important. In fact, these errors are negligible for small values of W. In Table VI, we present the error for each source and algorithm (version 2), taking into account all the cases with different values of W, ε, and $\Delta\varepsilon$ considered in this section. Similar results were obtained for version 1 of the algorithms.

V. VALIDATION

The errors presented in the previous section are only a theoretical estimation. A comparison between actual ground measurements of LST and satellite sensor estimates is needed to evaluate the error of these algorithms in real conditions. Few LST validation studies can be found in the literature (e.g., [14], [15], [19], [28], and [43]). The validation of LST algorithms is only possible for certain land surfaces with thermal homogeneity at various scales, from field of view of ground instruments to several kilometers. The preferable validation targets are inland waters or densely vegetated surfaces.

Coll *et al.* [14], [15] presented a flat and thermally homogeneous area of rice crops located close to Valencia, Spain, where ground LST measurements were taken concurrently with daytime and cloud-free MODIS and AATSR overpasses during the summers of 2002–2005. Moreover, a new campaign in 2006 brings new validation measurements. Table VII shows all the dates with their ground temperature T_g, W_0, θ, and brightness temperature T_i of both sensors. Ground temperature was acquired by using four intercalibrated TIR radiometers (two CIMEL CE312 and two Everest). In order to capture the spatial variability of surface temperature, each radiometer took measurements following different transects in the same area of 1 km^2. The temporal variability was considered, taking measurements 30 min around sensor overpasses, but only the average of 3 min around sensor overpass was considered as a ground measurement. All measures were corrected for emissivity effect. More details on the measurement procedure can be found in [14] and [15].

TABLE IV

COEFFICIENTS FOR α AND β ESTIMATION [(14) and (15)] WITH THEIR STATISTICAL ERRORS FOR ALL ALGORITHMS. ADJUSTMENT ERROR (σ_α AND σ_β, RESPECTIVELY) AND CORRELATION COEFFICIENT (R^2) FOR EACH ALGORITHM ARE SHOWN

	ASWn	ASWf	ADA11	ADA12	MSW
α_0(K)	52.57±0.14	55.2±0.3	57.00±0.17	64.5±0.2	45.99±0.13
α_1 (Kcm^{-1})	1.13±0.11	-4.4±0.2	1.57±0.12	-4.53±0.16	4.67±0.10
α_2 (Kcm^{-2})	-1.023±0.017	-0.70±0.04	-1.18±0.02	-0.71±0.02	-1.446±0.014
σ_α(K)	*5*	*6*	*4*	*5*	*5*
R^2	*0.979*	*0.959*	*0.985*	*0.978*	*0.974*
β_0(K)	79.2±0.2	64.6±0.4	111.6±0.3	110.3±0.4	160.5±0.3
β_1 (Kcm^{-1})	-11.06±0.06	-11.432±0.12	-17.62±0.07	-19.84±0.10	-25.75±0.08
σ_β(K)	*9*	*11*	*9*	*13*	*15*
R^2	*0.837*	*0.805*	*0.928*	*0.896*	*0.916*

TABLE V

VALUES OF ΔT AND T_i USED FOR THE SENSITIVITY ANALYSIS

W	ASWn (K)			ASWf (K)			ADA11 (K)			ADA12 (K)			MSW (K)		
(cm)	ΔT	T_1	T_2	ΔT	T_1	T_2	ΔT	T_1	T_2	ΔT	T_1	T_2	ΔT	T_1	T_2
1	0.9	12.5	11.6	1.3	11.0	9.7	0.7	10.0	9.4	1.1	9.0	7.9	0.3	9.5	9.3
2	1.9	19.0	17.2	2.7	19.0	16.3	1.5	20.0	18.5	2.0	19.0	17.1	0.9	19.0	18.2
3	2.5	26.0	23.5	3.4	24.0	20.6	2.0	26.0	24.1	3.0	23.0	20.0	1.5	26.0	24.5
4	3.3	29.0	25.8	4.0	28.0	24.1	2.9	24.5	21.7	3.6	22.5	18.9	1.9	24.0	22.2
5	3.8	25.0	21.2	4.5	23.0	18.6	3.3	24.0	20.7	4.0	22.0	18.1	2.2	24.0	21.8

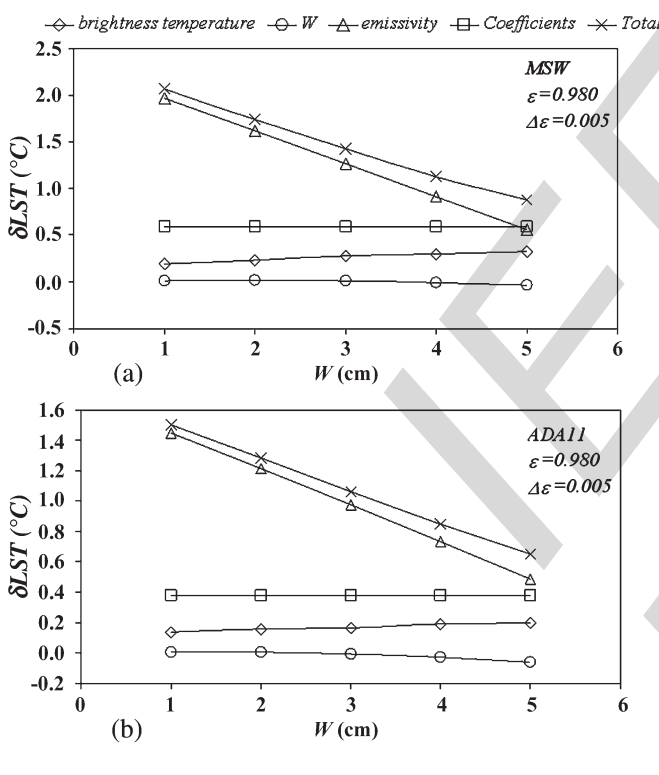

Fig. 7. Error in LST due to the different sources in the case of (a) MSW and (b) ADA11.

TABLE VI

ERRORS IN LST FOR ALL ERROR SOURCES FOR THE ALGORITHM OF VERSION 2 [WHEN α AND β COEFFICIENTS ARE OBTAINED BY USING (14) AND (15)]. THE LAST COLUMN SHOWS THE TOTAL LST ERROR OF THE ALGORITHM

	$\delta(T_i)$	$\delta(W)$	$\delta(\varepsilon, \Delta\varepsilon)$	δ(Coef.)	$\delta(T)$
ASWn	0.2	0.06	0.8	0.6	1.1
ASWf	0.2	0.10	0.6	1.3	1.5
ADA11	0.2	0.07	1.0	0.4	1.1
ADA12	0.2	0.09	0.9	0.8	1.3
MSW	0.3	0.09	1.4	0.6	1.5

To validate the MODIS algorithms, W_0 is obtained from MODIS atmospheric profile product (MOD07, [35]). For AATSR, a MOD07 product can be found in all cases with spatial concurrence and temporal difference less than 1 h, which can be used to validate our algorithms. The mean W_0 and standard deviation in all days was (2.4±0.5) cm.

Rice crops with full cover have a high emissivity and a low spectral variation. Surface emissivity was measured in the field using the box method [33] for the four-band CE312 CIMEL radiometer which has two bands that are similar to the AATSR channels at 11 and 12 μm. The measured mean emissivity and the spectral emissivity difference for AATSR nadir view (ASWn) were $\varepsilon = 0.983$ and $\Delta\varepsilon = 0.005$ [15], respectively. Those measurements are valid for nadir view only. Measurements of angular variations of emissivity in natural surfaces are scarce. Lagouarde *et al.* [21] measured the differences between nadir and off-nadir temperatures in several land surfaces. Specifically, for full cover alfalfa crops with the absence of water stress (i.e., similar to the rice crops), the difference between nadir and off-nadir ($\sim$60°) temperatures was within 0.5 K. Such a decrease of temperature is equivalent to an emissivity decrease about $\sim$0.01 between both observations. For this reason, we took the mean emissivity and the spectral emissivity difference for ASWf as $\varepsilon = 0.973$ and $\Delta\varepsilon = 0.005$, respectively. Analogously, we took $\varepsilon = 0.980$ and $\Delta\varepsilon = 0.010$ for ADA11 and $\varepsilon = 0.975$ and $\Delta\varepsilon = 0.010$ for ADA12. The emissivity for MSW is obtained through the LST and the emissivity operational product of MODIS (MOD11, [42]), which is based on a land-cover classification [35]. For the rice-crop area, it yielded mean emissivity and spectral emissivity difference of $\varepsilon = 0.983$ and $\Delta\varepsilon = -0.003$. T_i are obtained as the mean of 3×3 pixels centered in our validation site. Table VIII shows the obtained LST with all algorithms, and Table IX presents the

TABLE VII
VALIDATION DATES WITH THEIR GROUND TEMPERATURE T_g, W, θ, AND BRIGHTNESS TEMPERATURE T_i OF BOTH SENSORS (COLL *et al.* [14], [15]). NEW DATES ARE MARKED WITH $*$

			MODIS data			AATSR data					
Date	T_g (°C)	W_0(cm)	θ(°)	T_{31} (°C)	T_{32} (°C)	θ_n(°)	T_{11n} (°C)	T_{12n}(°C)	θ_f (°)	T_{11f} (°C)	T_{12f} (°C)
10-Jul-02	28.6±0.6	2.4				3.7	25.0	23.0	55.2	22.7	20.2
10-Jul-02	28.8±0.7	2.4	43.7	23.9	23.0						
13-Jul-02	27.6±0.9	2.3				13.8	22.3	19.3	54.2	19.2	15.7
26-Jul-02	27.9±0.6	3.5				1.1	23.4	20.7	55.2	20.8	17.7
8-Aug-02	26.5±0.7	2.9				16.2	20.3	17.3	53.9	17.4	13.9
14-Aug-02	28.5±0.5	2.7				3.9	23.7	21.5	55.2	21.2	18.6
17-Aug-02	29.1±0.6	2.6				13.9	22.8	19.8	54.2	20.5	16.9
5-Sep-02	28.0±0.8	1.9				19.1	24.1	22.0	53.3	22.9	20.2
8-Jul-03	28.3±0.7	2.2				11.1	25.3	23.0	54.6	23.0	20.3
11-Jul-03	29.1±0.7	1.6				1.2	27.0	25.5	55.2	25.1	23.4
11-Jul-03	28.9±0.8	1.6	27.7	26.7	26.2						
14-Jul-03	28.6±0.6	3.0				8.7	24.7	22.4	54.8	22.3	19.6
24-Jul-03	28.8±0.6	2.5				16.3	24.7	22.4	53.9	21.6	19.1
30-Jul-03	28.9±0.6	3.3				3.7	23.4	20.6	55.2	20.3	17.1
12-Aug-03	31.3±0.6	1.5				11.1	28.1	26.5	54.6	26.8	24.7
12-Aug-03	31.2±0.6	1.5	28.1	28.2	27.7						
28-Jun-04	29.2±0.6	2.4				8.7	26.4	24.4	54.8	23.7	21.4
8-Jul-04	25.7±0.6	1.9				16.3	23.2	21.6	53.8	21.3	19.3
8-Jul-04	25.3±0.6	1.9	50.3	22.5	21.9						
14-Jul-04	27.2±0.7	2.5				3.7	22.5	19.8	55.2	19.8	16.7
27-Jul-04	27.7±0.4	1.7				11.1	25.0	23.4	54.6	23.1	21.1
27-Jul-04	27.9±0.6	1.7	5.6	25.5	24.9						
30-Jul-04	27.8±0.4	3.3				1.2	23.4	20.6	55.2	20.4	16.9
3-Aug-04	30.0±0.7	2.4	6.2	26.8	26.0						
12-Aug-04	28.4±0.6	2.1				16.3	25.5	24.0	53.9	24.3	22.4
12-Aug-04	28.7±0.5	2.1	5.7	25.8	25.2						
12-Jul-05	27.0±0.6	2.2				11.1	24.6	23.0	54.6	23.0	21.0
12-Jul-05*	27.2±0.6	2.2	16.5	24.8	24.4						
14-Jul-05*	27.9±0.6	2.4	5.9	24.9	24.3						
21-Jul-05	28.5±0.6	2.0				19.0	25.4	23.6	53.3	23.7	21.6
21-Jul-05*	28.4±0.5	2.0	5.4	25.7	25.0						
28-Jul-05	28.8±0.5	2.7				16.3	24.8	22.7	53.8	22.3	19.9
28-Jul-05*	28.9±0.4	2.7	16.5	24.5	23.7						
6-Aug-05	28.0±0.5	1.8				13.7	25.4	23.7	54.3	24.0	21.9
6-Aug-05*	28.3±0.4	1.8	5.5	25.4	24.9						
3-Jul-06*	29.5±1.1	1.8				8.7	27.5	25.9	54.9	26.2	24.1
3-Jul-06*	29.9±0.9	1.8	27.6	27.5	27.1						
17-Jul-06*	29.9±0.7	2.9	6.0	25.0	23.7						
22-Jul-06*	29.5±0.6	2.4				13.7	26.4	24.4	54.2	24.6	22.2
22-Jul-06*	29.4±8	2.4	26.9	26.1	25.4						
24-Jul-06*	29.2±0.9	2.4	5.5	25.8	24.9						
28-Jul-06*	28.5±0.7	2.0	36.0	24.2	23.5						
2-Aug-06*	30.1±0.7	2.9	5.7	24.9	23.7						

statistics of the difference between the ground temperature and the LST. Although there are few data, skewness and kurtosis-3 factors are always less than unity, which means that the differences are normally distributed. Similar results are obtained for algorithms in version 1.

AQ6 ASWn and MSW have an rmse around 0.5 °C. ASWf is the SW algorithm with the largest rmse (±1.0 K); this is because it has large bias (0.6 K) and standard deviation ($\sigma = \pm 0.8$ K). The rmse of DA algorithms is near ±1.5 K in both cases. They show an underestimation of LST close to 1.0 K and a standard deviation larger than ±1.0 K. These errors make necessary further work in the study and characterization of the angular variation on emissivity. On the other hand, such errors could be also due to the differences in the atmospheric profiles along the paths of nadir and off-nadir views of AATSR.

VI. CONCLUSION

The CLAR database was presented to generate the LST retrieval algorithms from satellite sensor data. The radiosoundings of CLAR are well distributed in W being uniform up to 5.5 cm. They also have a good distribution in low, middle, and high latitudes (40%, 40%, and 20%, respectively). The first-layer temperature T_0 ranges from −20 °C to 40 °C. Five

TABLE VIII
LST FOR ALL THE VALIDATION DATES OBTAINED FOR THE ALGORITHMS GENERATED

Date	T_g *(°C)*	*MSW (°C)*	*ASWn (°C)*	*ASWf (°C)*	*ADA11 (°C)*	*ADA12 (°C)*
10-Jul-02	28.6±0.6		28.5	27.9	30.0	30.5
10-Jul-02	28.8±0.7	27.7				
13-Jul-02	27.6±0.9		28.0	27.3	29.2	29.5
26-Jul-02	27.9±0.6		28.3	27.5	29.0	28.7
8-Aug-02	26.5±0.7		25.9	25.3	26.7	26.6
14-Aug-02	28.5±0.5		27.4	26.5	29.0	29.4
17-Aug-02	29.1±0.6		28.4	28.8	27.7	27.6
5-Sep-02	28.0±0.8		27.6	28.4	26.6	26.5
8-Jul-03	28.3±0.7		29.3	28.7	30.1	30.2
11-Jul-03	29.1±0.7		29.6	28.6	30.9	30.9
11-Jul-03	28.9±0.8	29.4				
14-Jul-03	28.6±0.6		28.8	27.8	30.0	29.8
24-Jul-03	28.8±0.6		28.7	26.4	31.6	31.2
30-Jul-03	28.9±0.6		28.6	27.3	30.5	30.6
12-Aug-03	31.3±0.6		30.7	30.9	30.7	30.9
12-Aug-03	31.2±0.6	31.1				
28-Jun-04	29.2±0.6		29.9	28.2	32.4	32.4
8-Jul-04	25.7±0.6		25.7	25.2	27.0	27.4
8-Jul-04	25.3±0.6	25.2				
14-Jul-04	27.2±0.7		27.3	26.5	28.2	28.1
27-Jul-04	27.7±0.4		27.8	26.9	29.0	28.9
27-Jul-04	27.9±0.6	28.4				
30-Jul-04	27.8±0.4		28.5	28.2	30.0	30.9
3-Aug-04	30.0±0.7	30.4				
12-Aug-04	28.4±0.6		28.0	28.0	27.9	27.8
12-Aug-04	28.7±0.5	28.8				
12-Jul-05	27.0±0.6		27.3	26.8	28.1	28.1
12-Jul-05*	27.2±0.6	27.4				
14-Jul-05*	27.9±0.6	28.1				
21-Jul-05	28.5±0.6		28.4	27.7	29.0	28.7
21-Jul-05*	28.4±0.5	28.9				
28-Jul-05	28.8±0.5		28.3	27.0	30.0	29.9
28-Jul-05*	28.9±0.4	28.3				
6-Aug-05	28.0±0.5		28.1	28.0	28.1	28.0
6-Aug-05*	28.3±0.4	28.1				
3-Jul-06*	29.5±1.1		30.1	30.3	30.1	30.3
3-Jul-06*	29.9±0.9	30.2				
17-Jul-06*	29.9±0.7	30.3				
22-Jul-06*	29.5±0.6		29.7	29.4	30.0	30.0
22-Jul-06*	29.4±8	29.5				
24-Jul-06*	29.2±0.9	29.4				
28-Jul-06*	28.5±0.7	27.8				
2-Aug-06*	30.1±0.7	29.8				

different LST algorithms were generated with this database and using two different techniques: SW (one for MODIS and two for AATSR) and DA for AATSR. Different versions to obtain α and β coefficients were generated, obtaining similar results. Then, the fitting of α and β coefficients as a function of W could be a good approximation.

A sensitivity analysis was performed to evaluate all error sources for several values of mean emissivity and emissivity difference and W. The larger error for SW technique was ± 1.4 K (ASWf), and the minimum error was ± 0.8 K (ASWn), whereas MSW had an error of ± 0.9 K. In the case of DA, ADA11 had the minimum error (± 0.7 K), and ADA12 had the largest error (± 1.0 K).

The validation database of the Valencia test site (Coll *et al.* [14], [15]) was used to validate all these algorithms. The database was increased with new ground measurements and sensor data for 2006. The best results in terms of LST error were for ASWn (± 0.5 K) and MSW (± 0.4 K). These results confirm the conclusions shown by Coll *et al.* [14], [15]. The DA algorithms showed an error close to ± 1.5 K. Reasons for this discrepancy could be errors in the angular variation of surface emissivity. In fact, as shown in the sensitivity analysis, the main error source in these algorithms is due to the emissivity uncertainty. Moreover, the effect of the different spatial resolution and the difference in the atmospheric profiles between the nadir and off-nadir views of AATSR may be other sources of error.

TABLE IX
STATISTICS OF THE DIFFERENCE BETWEEN GROUND TEMPERATURE T_g AND LST T FOR THE ALGORITHMS GENERATED WITH VERSION 2. THE SIXTH LINE IS THE PERCENT OF CASES WHICH ARE INCLUDED IN THE RANGE $\bar{x} \pm$ s.d. FOR EACH CASE

	T_g-T				
	ASWn (K)	*ASWf (K)*	*ADA11 (K)*	*ADA12 (K)*	*MSW (K)*
Average $\bar{x}$	*0.0*	*0.6*	*-0.9*	*-1.0*	*0.0*
Standard deviation (s.d.)	*0.5*	*0.8*	*1.1*	*1.2*	*0.4*
RMSE	*0.5*	*1.0*	*1.5*	*1.6*	*0.4*
Maximum difference	*1.1*	*2.4*	*1.4*	*1.5*	*1.1*
Minimum difference	*-1.0*	*-0.8*	*-3.2*	*-3.2*	*-0.5*
% cases in ± s.d.	*64*	*68*	*72*	*72*	*72*
Skewness factor	*0.2*	*0.4*	*0.3*	*0.2*	*1.0*
Kurtosis-3 factor	*-0.7*	*-0.3*	*-0.3*	*-0.4*	*0.0*

ACKNOWLEDGMENT

The authors would like to thank the Department of Atmospheric Science, University of Wyoming, for the atmospheric radiosounding profiles. The authors would also like to thank the AATSR Validation Team, University of Leicester, European Space Agency under CAT-1 Project 3466 and the EOS-NASA under Project EOS/03-0043-0379 for providing the AATSR and MODIS data.

REFERENCES

[1] *AATSR Product Handbook*, ESA, Paris, France, Mar. 28, 2006. Issue 2.1, http://envisat.esa.int/ dataproducts/aatsr/

[2] M. R. Allen, C. T. Mutlow, G. M. C. Blumberg, J. R. Christy, R. T. McNider, and D. T. Llewellyn-Jones, "Global change detection," *Nature*, vol. 370, no. 6484, pp. 24–25, Jul. 1994.

[3] I. J. Barton, A. M. Zavody, D. O'Brein, D. R. Cutten, R. W. Saunders, and D. T. Llewellyn-Jones, "Theoretical algorithms for satellite-derived sea surface temperatures," *J. Geophys. Res.*, vol. 94, no. D3, pp. 3365–3375, Mar. 1989.

[4] F. Becker and Z.-L. Li, "Towards a local split-window method over land surfaces," *Int. J. Remote Sens.*, vol. 11, no. 3, pp. 369–394, 1990a.

[5] F. Becker and Z.-L. Li, "Temperature-independent spectral indices in thermal infrared bands," *Remote Sens. Environ.*, vol. 32, no. 1, pp. 17–33, Apr. 1990b.

[6] F. Becker and Z.-L. Li, "Surface temperature and emissivity at various scales: Definition, measurement and related problems," *Remote Sens. Environ.*, vol. 12, pp. 225–253, 1995.

[7] A. Berk, G. P. Anderson, P. K. Acharya, J. H. Chetwynd, L. S. Bernstein, E. P. Shettle, M. W. Matthew, and J. H. Adler-Golden, *MODTRAN 4 Users Manual*. Hascom AFB, MA: Air Force Res. Lab. Space Vehicles Directorate, 1999. report.

[8] A. Calle, J. L. Casanova, and C. Moclán, "Detection and monitoring of forest fires in China through the ENVISAT-AATSR sensor," in *Proc. 5th Int. Workshop Remote Sens. GIS Appl. Forest Fire Manage.: Fire Effects Assessment*, 2005, pp. 149–152.

[9] V. Caselles and J. A Sobrino, "Determination of frosts in orange groves from NOAA-9 AVHRR data," *Remote Sens. Environ.*, vol. 29, no. 2, pp. 135–146, Aug. 1989.

[10] V. Caselles, E. Valor, C. Coll, and E. Rubio, "Thermal band selection for the PRISM instrument. 1. Analysis of emissivity-temperature separation algorithms," *J. Geophys. Res.*, vol. 102, no. D10, pp. 11 145–11 164, May 1997.

[11] Y. Chemin and K. Honda, "Spatiotemporal fusion of rice actual evapotranspiration with genetic algorithms and an agrohydrological model," *IEEE Trans. Geosci. Remote Sens.*, vol. 44, no. 11, pp. 3462–3469, Nov. 2006.

[12] C. Coll, C. Caselles, J. A. Sobrino, and E. Valor, "On the atmospheric dependence of the split-window equation for land surface temperature," *Int. J. Remote Sens.*, vol. 15, no. 1, pp. 1915–1932, 1994.

[13] C. Coll and V. Caselles, "A split-window algorithm for land surface temperature from Advance Very High Resolution Radiometer data: Validation and algorithm comparison," *J. Geophys. Res.*, vol. 102, no. D14, pp. 16 697–16 713, 1997.

[14] C. Coll, V. Caselles, J. M. Galve, E. Valor, R. Niclòs, J. M. Sánchez, and R. Rivas, "Ground measurements for the validation of land surface temperatures derived from AATSR and MODIS data," *Remote Sens. Environ.*, vol. 97, no. 3, pp. 288–300, Aug. 2005.

[15] C. Coll, V. Caselles, J. M. Galve, E. Valor, R. Niclòs, and J. M. Sánchez, "Evaluation of split-window and dual-angle correction methods for land surface temperature retrieval from Envisat/AATSR data," *J. Geophys. Res.*, vol. 111, no. D12, p. 12 105, 2006. DOI:10.1029/2005JD006830.

[16] C. François, A. Brisson, P. Le Borgne, and A. Marsouin, "Definition of a radiosounding database for sea surface brightness temperature simulations. Application to sea surface temperature retrieval algorithm determination," *Remote Sens. Environ.*, vol. 81, no. 2/3, pp. 309–326, Aug. 2002.

[17] A. R. Gillespie, T. Matsunaga, S. Rokugawa, S. Hook, J. S. Cothern, and A. B. Kahle, "A Temperature and emissivity separation algorithm from Advance Spaceborne Thermal Emission and Reflection Radiometer (ASTER) images," *IEEE Trans. Geosci. Remote Sens.*, vol. 36, no. 4, pp. 1113–1125, Jul. 1998.

[18] J.-P. Goutorbe, T. Level, and A. Tinga *et al.*, "HAPEX-Sahel: A large scale study of land-atmosphere interactions in semi-arid tropics," *Ann. Geophys.*, vol. 12, no. 1, pp. 53–64, Jan. 1993.

[19] S. Hook, R. Vaughan, H. Tonooka, and S. Schladow, "Absolute radiometric in-flight validation of mid and thermal infrared data from ASTER and MODIS using the Lake Tahoe CA/NV, USA automated validation site," *IEEE Trans. Geosci. Remote Sens.*, vol. 45, no. 6, pp. 1798–1807, Jun. 2007.

[20] Y. H. Kerr, J. P. Lagouarde, and J. Imbernon, "Accurate land surface temperature retrieval from AVHRR data with use of an improved split window algorithm," *Remote Sens. Environ.*, vol. 41, no. 2/3, pp. 197–209, Aug./Sep. 1992.

[21] J. P. Lagouarde, Y. H. Kerr, and Y. Brunet, "An experimental study of angular effects on surface temperature for various plant canopies and bare soils," *Agric. For. Meteorol.*, vol. 77, no. 3/4, pp. 167–190, Dec. 1995.

[22] E. F. Lambin and D. Ehrlich, "Land-cover changes in sub-Saharan Africa (1982–1991): Application of a change index based on remotely sensed surface temperature and vegetation indices at a continental scale," *Remote Sens. Environ.*, vol. 61, no. 2, pp. 181–200, Aug. 1997.

[23] G. Laneve, M. M. Castronuovo, and E. G. Cadau, "Continuous monitoring of forest fires in the Mediterranean area using MSG," *IEEE Trans. Geosci. Remote Sens.*, vol. 44, no. 10, pp. 2761–2768, Oct. 2006.

[24] L. M. McMillin, "Estimation of sea surface temperatures from two infrared window measurements with different absorption," *J. Geophys. Res.*, vol. 80, no. C36, pp. 5113–5117, 1975.

[25] F. Nerry, F. Petitcolin, and M. D. Stoll, "Bidirectional reflectivity in AVHRR channel 3: Application to a region in northern Africa," *Remote Sens. Environ.*, vol. 66, no. 3, pp. 298–316, Dec. 1998.

[26] H. Ouaidrari, S. N. Goward, K. P. Czajkowski, J. A. Sobrino, and E. Vermonte, "Land surface temperature estimation from AVHRR thermal infrared measurements. An assessment for AVHRR Land Pathfinder II data set," *Remote Sens. Environ.*, vol. 81, no. 1, pp. 114–128, Jul. 2002.

[27] A. C. Pinheiro, J. Privette, R. Mahoney, and C. J Tucker, "Directional effects in a daily AVHRR land surface temperature dataset over Africa," *IEEE Trans. Geosci. Remote Sens.*, vol. 42, no. 9, pp. 1941–1954, Sep. 2004.

[28] A. J. Prata, "Land surface temperatures derived from the advanced very high resolution radiometer and the along track scanning radiometer 2. Experimental results and validation of AVHRR algorithms," *J. Geophys. Res.*, vol. 99, no. D6, pp. 13 025–13 058, 1994.

[29] A. J. Prata and R. P. Cechet, "An assessment of the accuracy of land surface temperature determination from the GMS-5 VISSR," *Remote Sens. Environ.*, vol. 67, no. 1, pp. 1–14, Jan. 1999.

[30] A. J. Prata, "Land surface temperature measurement from space: AATSR algorithm theoretical basis document," CSIRO Atmos. Res., Aspendale, Australia, Tech. Rep. 34, 2002.

[31] J. C. Price, "Land surface temperature measurements from the splitwindow channels of the NOAA 7 AVHRR," *J. Geophys. Res.*, vol. 89, no. D5, pp. 7231–7237, 1984.

[32] E. Rubio, V. Caselles, and C. Badenas, "Emissivity measurements of several soils and vegetation types in the 8–14 μm wave band: Analysis of two field methods," *Remote Sens. Environ.*, vol. 59, no. 3, pp. 490–521, Mar. 1997.

[33] E. Rubio, V. Caselles, C. Coll, E. Valor, and F. Sospedra, "Thermal-infrared emissivities of natural surfaces: Improvements on the experimental set-up and new measurements," *Int. J. Remote Sens.*, vol. 24, no. 24, pp. 5379–5390, Dec. 2003.

[34] B. Seguin, F. Becker, T. Phulpon, X. F. Gu, G. Guyot, Y. Kerr, C. King, J. P. Lagouarde, C. Ottlé, M. P. Stoll, and A. Tabbagh, "IRSUTE: A Minisatellite Project for land surface heat flux estimation from field to regional scale," *Remote Sens. Environ.*, vol. 68, no. 3, pp. 357–369, Jun. 1999.

[35] S. W. Seemann, E. E. Borbas, J. Li, W. P. Menzel, and L. E. Gumley, *MODIS Atmospheric Profile Retrieval Algorithm Theoretical Basis Document*. Madison, WI: Univ. Wisconsin-Madison, 2006. 40 pp.

[36] W. C. Snyder and Z. Wan, "BRDF model to predict spectral reflectance and emissivity in the thermal infrared," *IEEE Trans. Remote Sens.*, vol. 36, no. 1, pp. 214–225, Jan. 1998.

[37] G. N. Toller and A. Isaacman, *MODIS Level 1B Product User's Guide*. Greenbelt, MD: NASA/Gooddard Space Flight Center, 2003.

[38] E. Valor and V. Caselles, "Mapping land surface emissivity from NDVI: Application to European, African, and South American areas," *Remote Sens. Environ.*, vol. 57, no. 3, pp. 167–184, Sep. 1996.

[39] A. A. Van de Griend and M. Owe, "On the relationship between thermal emissivity and the normalized difference vegetation index for natural surfaces," *Int. J. Remote Sens.*, vol. 14, no. 6, pp. 1119–1131, 1993.

[40] Z. Wan and J. Dozier, "Land-surface temperature measurement from space: Physical principles and inverse modeling," *IEEE Trans. Geosci. Remote Sens.*, vol. 27, no. 3, pp. 268–277, May 1989.

[41] Z. Wan and J. Dozier, "A generalized split-window algorithm for retrieving land-surface temperature from space," *IEEE Trans. Geosci. Remote Sens.*, vol. 34, no. 4, pp. 892–905, Jul. 1996.

[42] Z. Wan, *MODIS Land Surface Temperature. Algorithm theoretical basis document*, 1999. NAS5-31370.

[43] Z. Wan, Y. Zhang, Q. Zhang, and Z.-L. Li, "Validation of the land surface temperature products retrieved from TERRA MODerate resolution Imaging Spectroradiometer data," *Remote Sens. Environ.*, vol. 83, no. 1/2, pp. 163–180, Nov. 2002.

[44] F. Yang, M. A. White, A. R. Michaelis, K. Ichii, H. Hashimoto, P. Votava, A-X. Zhu, and R. R. Nemani, "Prediction of continental-scale evapotranspiration by combining MODIS and AmeriFlux data through support vector machine," *IEEE Trans. Geosci. Remote Sens.*, vol. 44, no. 11, pp. 3452–3461, Nov. 2006.

[45] Y. Yu, J. L. Privette, and A. C. Pinheiro, "Analysis of the NPOESS VIIRS land surface temperature algorithm using MODIS data," *IEEE Trans. Geosci. Remote Sens.*, vol. 43, no. 10, pp. 2340–2350, Oct. 2005.

Joan M. Galve was born in July 1978, in Benifaio, Valencia, Spain. He received the B.Sc. degree in physics and the M.Sc. degree in earth physics and thermodynamics from the University of Valencia, Valencia, in 2004 and 2006, respectively, where he is currently working toward the Ph.D. degree in earth physics and thermodynamics in the Department of Earth Physics and Thermodynamics, Faculty of AQ7 Physics.

César Coll received the B.Sc., M.Sc., and Ph.D. degrees in physics from the University of Valencia, Valencia, Spain, in 1989, 1992, and 1994, respectively.

He is currently an Associate Professor of earth physics with the Department of Earth Physics and Thermodynamics, Faculty of Physics, University AQ8 of Valencia. His research interest focuses on the physical processes of thermal-infrared (TIR) remote sensing, atmospheric and emissivity corrections, temperature-emissivity separation, and ground validation of Advanced Along Track Scanning Radiometer, Moderate Resolution Imaging Spectroradiometer, and Advance Spaceborne Thermal Emission and Reflection Radiometer TIR products. He has published 40 papers in AQ9 international journals and 50 conference papers.

Vicente Caselles AQ10

He is a Professor of applied physics and the Head of the Thermal Remote Sensing Group, Department of Earth Physics and Thermodynamics, Faculty of Physics, University of Valencia, Valencia, Spain. AQ11 He has an expertise of 30 years in the physical processes involved in the temperature measurement using remote-sensing techniques, which has been documented through 10 books, 20 doctoral theses, 100 papers in international journals, 60 conference papers, and 30 reports.

Prof. Caselles was collaborating with the ESA as a member of the Advisory Group for the Land-Surface Processes and Interactions Mission. He was the Chairman of the Spanish Remote Sensing Society, and he is currently the Manager of the Spanish Atmosphere and Climate Programme.

Enric Valor received the B.Sc. and Ph.D. degrees in physics from the University of Valencia, Valencia, Spain, in 1992 and 1997, respectively.

He is currently an Associate Professor of earth physics with the Department of Earth Physics and Thermodynamics, Faculty of Physics, University AQ12 of Valencia. His research interest focuses on the physical processes of thermal-infrared remote sensing, emissivity measurement and characterization, atmospheric and emissivity corrections, and temperature-emissivity separation algorithms. He has published 35 papers in international journals and 45 conference papers.

AUTHOR QUERIES

AUTHOR PLEASE ANSWER ALL QUERIES

AQ1 = Please provide the specific "institution or organization" that supported the work of "J. M. Galve."
AQ2 = "Wan and Dozier [27] was changed to "Pinheiro et al. [27]" based on the reference list. Please check if appropriate.
AQ3 = The acronym "TES" was defined as "temperature emissivity separation." Please check if appropriate.
AQ4 = The acronym "TISI" was defined as "temperature-independent spectral indices." Please check if appropriate.
AQ5 = The acronym "IGBP" was defined as "International Geosphere-Biosphere Programme." Please check if appropriate.
AQ6 = "root minimum square error" was changed to "root mean square error" or "rmse." Please check if appropriate.
AQ7 = The complete current affiliation of "Joan M. Galve" was provided in the curriculum vitae based on the affiliation footnote. Please check if appropriate.
AQ8 = The complete current affiliation of "César Coll" was provided in the curriculum vitae based on the affiliation footnote. Please check if appropriate.
AQ9 = The acronym "ASTER" was defined as "Advance Spaceborne Thermal Emission and Reflection Radiometer." Please check if appropriate.
AQ10 = Please provide the educational background of "Vicente Caselles."
AQ11 = The complete current affiliation of "Vicente Caselles" was provided in the curriculum vitae based on the affiliation footnote. Please check if appropriate.
AQ12 = The complete current affiliation of "Enric Valor" was provided in the curriculum vitae based on the affiliation footnote. Please check if appropriate.

Note: 1) Changes were made in Ref. [17]. Please check if appropriate.

ATTN: If you are paying to have all or some of your figures appear in color in the print issue, it is very important that you fill out and submit a copy of the IEEE Page Charge & Reprint Form along with your proof corrections. This form is available from the same URL where these page proofs were downloaded from. Thank you

END OF ALL QUERIES